Synthesis and Structure of a Two-Dimensional Palladium Oxide Network on Reduced Graphene Oxide

Zheng, Zhiyong; Cao, Huili; Meng, Jie; Xiao, Yong; Ulstrup, Jens; Zhang, Jingdong; Zhao, Feng; Engelbrekt, Christian; Xiao, Xinxin

Published in:
Nano Letters

Link to article, DOI:
10.1021/acs.nanolett.2c01226

Publication date:
2022

Document Version
Peer reviewed version

Cite the paper: https://pubs.acs.org/doi/full/10.1021/acs.nanolett.2c01226

Synthesis and Structure of a Two-Dimensional Palladium Oxide Network on Reduced Graphene Oxide

Zhiyong Zheng[1], Huili Cao[1], Jie Meng[1], Yong Xiao[2], Jens Ulstrup[1], Jingdong Zhang[1,¶], Feng Zhao[2], Christian Engelbrekt[1]*, Xinxin Xiao[1]**

[1]Department of Chemistry, Technical University of Denmark, Kemitorvet, Building 207, Kongens Lyngby, DK-2800, Denmark

[2]CAS Key Laboratory of Urban Pollutant Conversion, Institute of Urban Environment, Chinese Academy of Sciences, 1799 Jimei Road, Xiamen, 361021, China

KEYWORDS: superlattice, *S. oneidensis* MR-1, biosynthesis, palladium oxide, graphene

ABSTRACT: New nanostructures often reflect new and exciting properties. Here, we present a hitherto unreported two-dimensional PdO square network with lateral dimensions up to hundreds of nanometers growing on reduced graphene oxide (rGO), forming a hybrid nanofilm. An intermediate state of dissolved Pd(0) in the bacterium *S. oneidensis* MR-1 is pivotal in the

biosynthesis and inspires an abiotic synthesis. The PdO network shows a lattice spacing of 0.5 nm and a thickness of 1.8 nm on both sides of an rGO layer and is proposed to be cubic or tetragonal crystal, as confirmed by structural simulations. A 2D silver oxide analog with a similar structure is also obtained using an analogous abiotic synthesis. Our study thus opens a simple route to a whole new class of 2D metal oxides on rGO as promising candidates for graphene superlattices with unexplored properties and potential applications for example in electronics, sensing, and energy conversion.

New structures often possess novel physicochemical properties of exceptional interest.[1-4] As an emerging graphene derivative, graphene superlattices have attracted considerable attention due to their great potential in applications of electric and optical devices.[5-6] Research focus has been devoted particularly to two subgroups, i.e., magic-angle graphene superlattices and graphene/hexagonal boron-nitride superlattices,[5-12] while the interaction of graphene with other crystal layers has rarely been reported. Unexpected structures and properties were reported when graphene oxide (GO) was decorated with metal nanomaterials,[13-16] which implies uncharted interactions between the metals and GO. For example, a PdO interlayer was formed following the interaction between Pd atoms and GO, leading to unusual 2D-like growth, while Ag, Au, and Pt grew randomly on GO. The Pd-decorated GO showed good performance in gas sensing and electrochemical water splitting.[13] Ir/Pd nanocluster superlattices with high structural perfection

were formed when Ir and Pd were deposited successively on a graphene/Ir(111) substrate, exhibiting great hydrogen solubility for hydrogen storage.[17] However, to the best of our knowledge, a homogeneous metallic crystal layer on graphene alongside new properties has not been reported.

Biogenic metal nanomaterials have shown exclusive properties. For example, Pd nanoparticles (PdNPs) produced by *S. oneidensis* MR-1 (MR-1) selectively catalyzes the oxidation of formate over other small organic molecules, while the unique selectivity was absent in the electrochemically deposited Pd.[18] Arsenic-sulfide nanotubes synthesized by *Shewanella* sp. HN-41 displayed decreased electrical conductance with increasing temperature like a metal, but was simultaneously photoactive like a semiconductor.[1] These exclusive properties are believed to result from the unusual structure and/or composition originating from interactions between microbes and metals.[19] Nevertheless, biosynthesis is typically limited by its low yield and poor control. Understanding the unique interplay between microbes and metals would not only unveil the operating mechanism of the microbe exposed to extracellular metals,[20-24] but guide analogous abiotic synthesis with often easier control and a higher yield.[25-28]

We report here the synthesis and structure of a 2D PdO square network on a reduced GO (rGO) layer. The PdO network completely and homogeneously covers both sides of the rGO layer, leading to a hybrid nanofilm. The nanofilm was initially discovered in a biosynthesis process, in which dissolved Pd(0), as an intermediate form of Pd(II) towards PdNPs during the microbial reduction by MR-1, is released from MR-1 cells to the GO surface where the network is formed

and GO reduced to rGO in a following hydrothermal process. Control experiments suggest that the dissolved Pd(0) is the key to the network formation, inspiring an abiotic synthesis of the same structure, in which the role of MR-1 is taken by $K_4[Fe(CN)_6]$ to produce dissolved Pd(0). The network is validated to be PdO by elemental analysis. Further investigations by microscopies show a thickness of 1.8 nm on each side of the rGO layer and a lattice spacing of 0.5 nm of the PdO network. An unprecedented crystal structure (cubic or tetragonal) of PdO is proposed and matches well all the results. A hitherto unreported and similar rGO-based silver oxide nanofilm is also prepared from the abiotic synthesis. The common square network of metal oxides on the rGO layer is proposed to be a consequence of the strong surface energy of the rGO layer, rather than the weak interaction within PdO crystal that originates from the large spacing, and is supported by a lattice matching model between metal oxides and rGO. Our study thus indicates a novel interaction between transition metal oxides and rGO and offers a potentially simple wet chemical method for graphene superlattice preparation.

To prepare the biosynthesis product (S-Pd-GO), a Pd(II) source and GO were incubated with *S. oneidensis* MR-1 (MR-1), followed by a hydrothermal process (Scheme 1a, details in Supporting Information). With a lateral dimension of up to 800 nm, the S-Pd-GO layer ("S" stands for *S. oneidensis* MR-1) displayed a film morphology analogous to that of GO and rGO (Figure 1a). The fast Fourier transform (FFT) of transmission electron microscopy (TEM) images disclosed a lattice spacing of 0.5 nm (Figure 1a) which, however, matches neither that of GO nor of rGO. High-

resolution TEM (HRTEM) showed instead a square network structure of the nanofilm with a lattice spacing of 0.5 nm and interplanar angles of 90° (Figure 1b and c), further confirming that the network is neither GO nor rGO. A large number of nanoparticles with higher contrast on the nanofilm can be also observed (Figure 1b). The network structure (dark background) and nanoparticles (bright spots) exhibited distinctive contrasts in scanning TEM (STEM) (Figure 1d). In previous work, MR-1 cells were wrapped by rGO decorated by PdAu alloy nanoparticles when Pd(II) and Au(III) were reduced by MR-1 and treated by a hydrothermal process.[14] In the present work, MR-1 cells were completely enveloped by the square network (Figure S2), rather than by rGO. It can therefore be suggested that the rGO is completely covered by the square network.

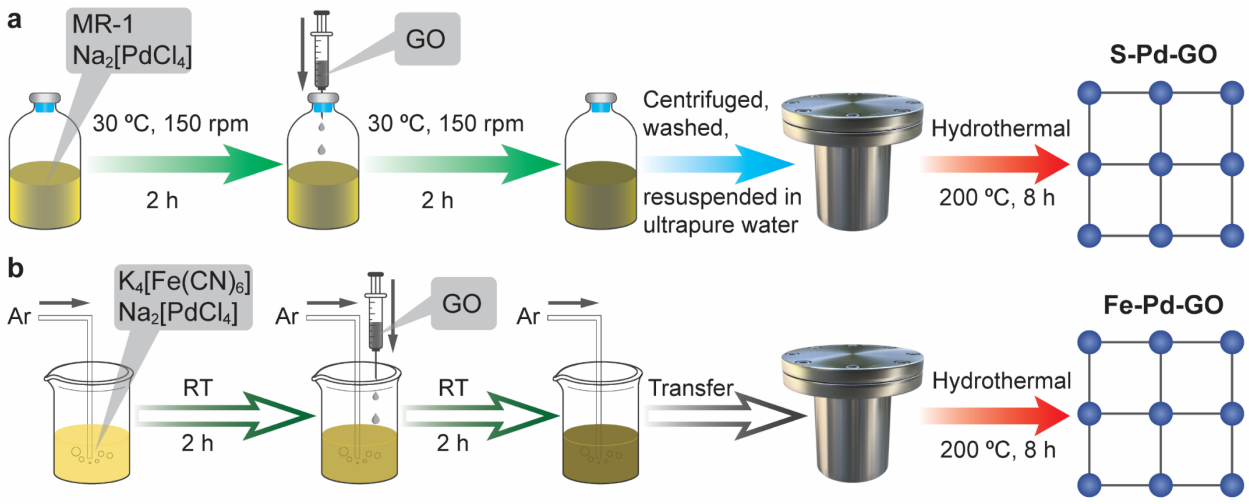

Scheme 1. Synthesis routes of the rGO-based nanofilm. (a) Biosynthesis of nanofilm S-Pd-GO with *S. oneidensis* MR-1 (MR-1), $Na_2[PdCl_4]$, and graphene oxide (GO). Unless otherwise stated, S-Pd-GO and other sample designations refer specifically to the rGO-based film structures. (b)

Bioinspired analogous abiotic synthesis of nanofilm Fe-Pd-GO ("Fe" for $[Fe(CN)_6]^{4-}$) with $K_4[Fe(CN)_6]$, $Na_2[PdCl_4]$, and GO. RT: room temperature.

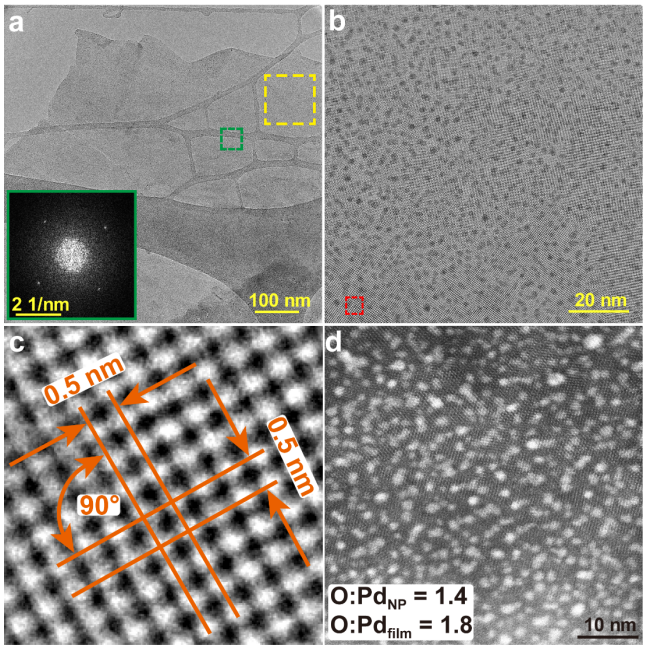

Figure 1. Morphology and elemental composition of S-Pd-GO. (a) TEM of S-Pd-GO with lateral dimensions up to 800 nm. Inset: FFT of the green square area. A large-size TEM image is shown in Figure S1. (b) HRTEM of the yellow square area in (a). (c) Enlarged view of the red square area in (b) showing a lattice spacing of 0.5 nm and interplanar angles of 90°. (d) High-resolution STEM image showing homogeneous distribution of nanoparticles on the nanofilm. Inset white box: Atomic ratio (O:Pd) of nanoparticle and nanofilm characterized by STEM-equipped EDS point analysis.

The elemental compositions of nanoparticles and nanofilm were characterized by energy-dispersive X-ray spectroscopy (EDS) in STEM mode. Only palladium and oxygen signals were

detected on both nanoparticles and nanofilm, with an atomic ratio of oxygen to palladium of 1.4 and 1.8, respectively (inset of Figure 1d). It is obvious that the nanofilm contains more oxygen than the nanoparticles alone. The EDS data show that the nanofilm is most likely palladium(II) oxide considering the contribution from adsorbed oxygen on the sample and residual oxygen in the TEM column. Two phases of palladium oxide (PdO and Pd_2O) have been reported,[29-31] but more data are yet required to validate Pd_2O. We therefore attribute the square network to PdO. It is well-known that MR-1 can reduce Pd(II) and produce Pd nanoparticles (PdNPs),[14, 18, 32-33] the HRTEM structure of which matches Pd(0) (Figure S3).[34] Hence the nanoparticles are concluded to be PdNPs. Another possible source of PdNPs found in the TEM images can be the reduction of the PdO square network triggered by the TEM electron beam. Of note, the square network and nanoparticles were not in the same plane, as confirmed by TEM images recorded at different focus values (Figure S4).

Control experiments were carried out to further investigate the square network formation. The hydrothermal process is essential for the formation of the square network, as evidenced by the TEM of S+Pd+GO (the precursor of S-Pd-GO prior to the hydrothermal process), which only shows GO film coated with a few PdNPs (Figure S5). To study the role of MR-1, synthesis without MR-1 cells was attempted (Scheme S1a). This product (Pd-GO) was a random mixture of rGO and PdNPs, showing no square network structure (Figure S6a). The reduction of Pd(II) to PdNPs (with MR-1 absent) and GO to rGO therefore takes place during the hydrothermal process, although no reducing chemical agent was introduced. However, the hydrothermal Pd(II) reduction

here did not lead to the square network formation. Both Pd(II) reduction by MR-1 in the presence of GO and the hydrothermal process are therefore essential for generating the square network.

It is known that MR-1 reduces Pd(II) to Pd(0) in the periplasm, where the PdNPs are thus formed.[32, 35-36] There are two fractions of Pd species before GO is added in the synthesis of S-Pd-GO: one is associated with MR-1 cells, the other one is in the bulk solution. To ascertain their separate roles in the square network formation, the two Pd fractions were separated by centrifugation into supernatant and pellet before GO addition, resulting in S-Pd_CS-GO and S-Pd_CP-GO respectively (Scheme S1b, "CS" and "CP" for centrifugation supernatant and centrifugation pellet, respectively). No square network formed, and only rGO with a homogeneous coating of PdNPs was observed for both S-Pd_CS-GO and S-Pd_CP-GO (Figure S6b and c). This suggests that both Pd species are essential in the formation of the square network. These control experiments also prove that PdNPs on GO themselves will not generate the square network.

A formation mechanism for the square network in S-Pd-GO is proposed (Figure S7). Pd(II) is taken up by MR-1 and reduced to Pd(0) in the periplasm. The initial Pd(0) is in the form of either dissolved Pd(0) atoms, small Pd(0) nanoclusters, or larger PdNPs (Figure S7a and b). During the hydrothermal process, the unbound Pd(0) atoms are released from the periplasm and oxidized by GO, followed by PdO deposition growing along preferred orientation and forming the square network on rGO (Figure S7c). The presence of dissolved Pd(0) atoms (or Pd(0) nanoclusters) is the key to the network formation. Proper experimental conditions, *e.g.*, a mild temperature, are thus essential to prevent further evolution of the dissolved Pd(0) atoms to PdNPs before the

hydrothermal process. The dissolved state of Pd(0) atoms or clusters is evidenced by the extracellular presence of PdNPs from Pd(II) reduction by MR-1 in the periplasm at ambient temperature.[32, 37] The Pd(0) membrane permeability was accelerated in the hydrothermal process. The presence of Pd(II) in the bulk media two hours after GO addition is important to ensure continuous Pd(II) reduction to Pd(0).

To validate the proposed mechanism and simplify the synthesis, an abiotic synthesis, in which MR-1 was replaced by the reducing reagent $K_4[Fe(CN)_6]$ was designed. This product is labeled Fe-Pd-GO (Scheme 1b). As displayed in Figure 2a to e, the morphology of Fe-Pd-GO regarding lattice spacing and interplanar angles is the same as that of S-Pd-GO, except that fewer PdNPs were found on the nanofilm. With the product not being associated with MR-1 cells, the thickness of Fe-Pd-GO and GO was measured to be 4.6 nm (Figure 2f) and 1 nm (Figure S10), respectively, by atomic force microscopy (AFM). The nanofilm seems to consist of a layer of rGO with 1.8 nm of square network on both sides. Note that the Fe-Pd-GO surface is very smooth as indicated by AFM (Figure 2f), with few particles in TEM and STEM images (Figure 2a-e). This could suggest that the electron beam of the TEM and STEM induces partial reduction of pristine S-Pd-GO and Fe-Pd-GO forming PdNPs. This is supported by a control experiment showing that PdNPs develop to a larger size with the TEM irradiation time (Figure S11).

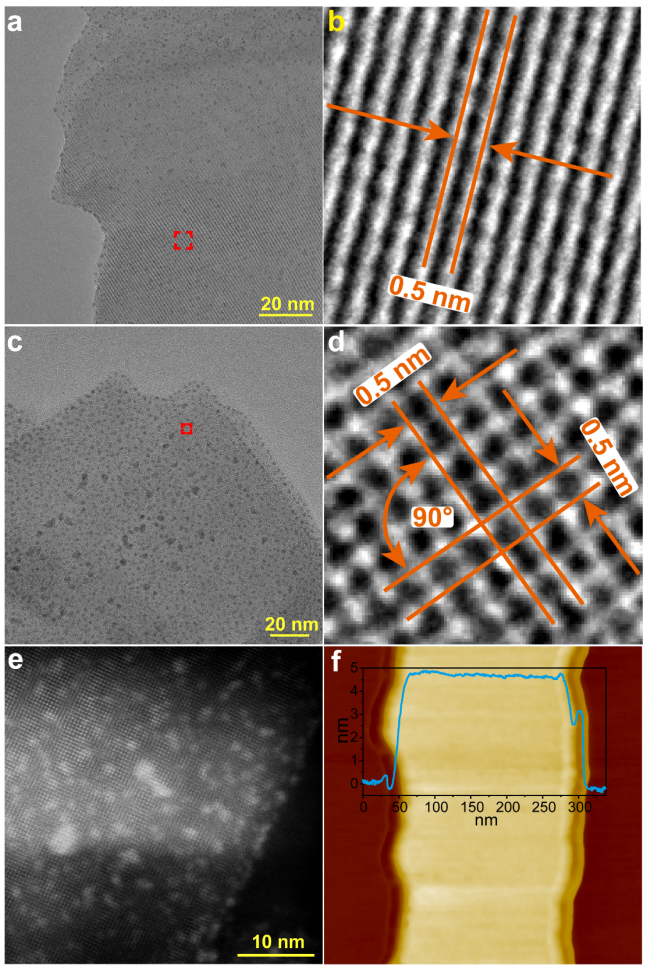

Figure 2. Morphology of Fe-Pd-GO. (a) TEM, (b) enlarged view of the red square area in (a), (c) HRTEM, (d) enlarged view of the red square area in (c), (e) high-resolution STEM, and (f) AFM topography image and typical height-profile along the cyan line. Large-size TEM images are shown in Figure S8 and Figure S9.

The composition and structure of S-Pd-GO and Fe-Pd-GO were further studied. As expected, only Pd(0) peaks were found in the Pd 3d spectrum using X-ray photoelectron spectroscopy (XPS) on S+Pd+GO, while both Pd(0) and PdO peaks appeared on S-Pd-GO and Fe-Pd-GO (Figure 3a-c). This further supports that the square network is PdO and not Pd_2O. In S-Pd-GO, 31.3% of Pd

is in the Pd(0) state, but only 7.1% in Fe-Pd-GO. This is likely due to the stronger reducing ability of MR-1 over $K_4[Fe(CN)_6]$. Of note, X-ray exposure can reduce PdO to Pd(0), which explains the presence of Pd(0) in the XPS of Fe-Pd-GO. X-ray diffraction (XRD) patterns of S-Pd-GO and Fe-Pd-GO are also similar with dominant 2θ peaks of 17.7°, 26.1°, 35.9°, and 40.3° (Figure 3d). To the best of our knowledge, no existing XRD pattern in the library matches the PdO pattern from the present work, suggesting that a new structure has been produced. S+Pd+GO and Fe+Pd+GO showed two 2θ peaks at 11.1° and 42.3° belonging to GO (Figure S12), again highlighting that the nanofilm formed during the hydrothermal process. Selected area electron diffraction (SAED) of the nanofilm displayed a single crystal pattern (Figure 3e), according with the SAED and HRTEM results (Figure 1 and Figure 2).

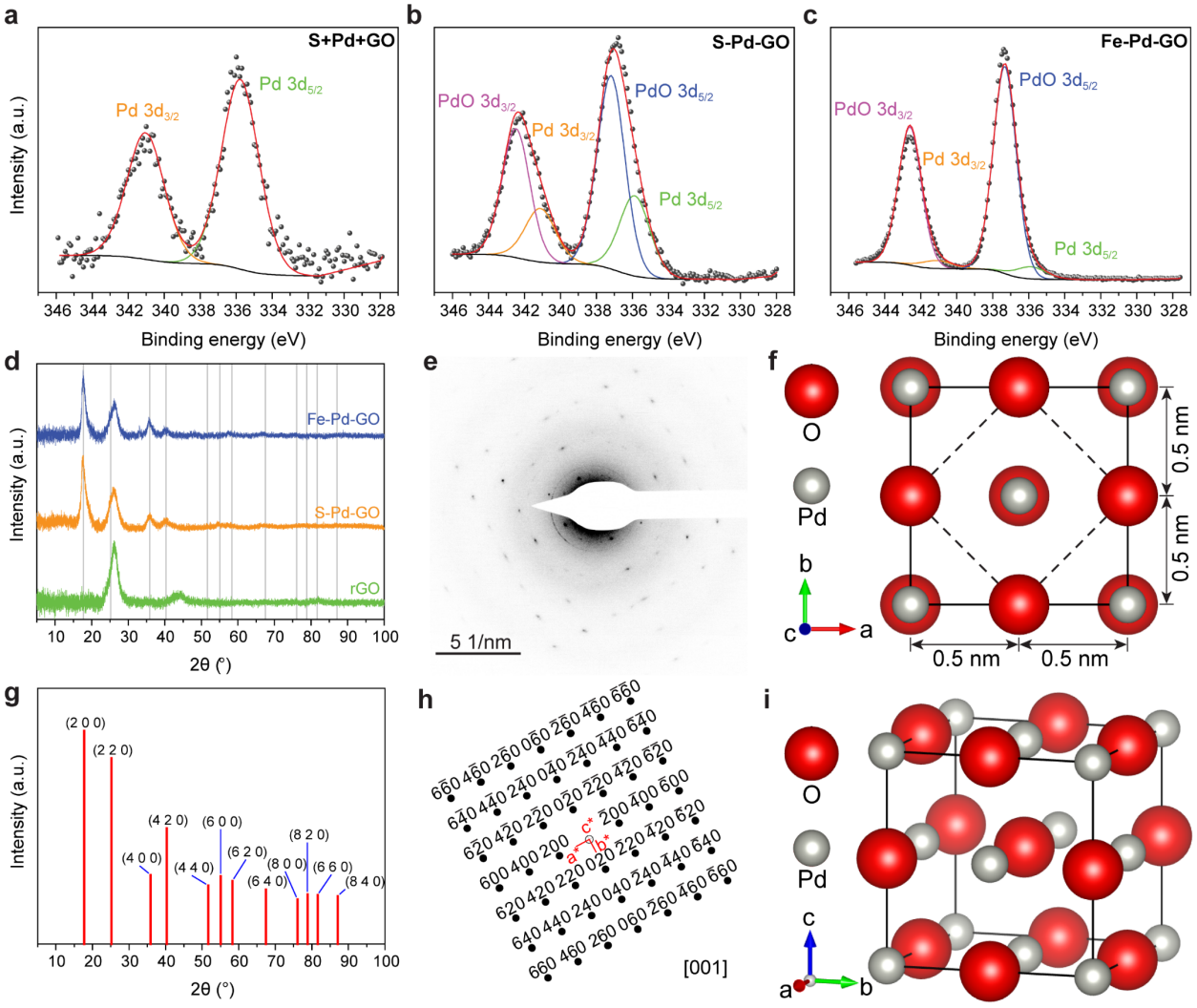

Figure 3. Composition and proposed structure of the nanofilm. High-resolution Pd 3d XPS of (a) S+Pd+GO, the precursor of S-Pd-GO before the hydrothermal process, (b) S-Pd-GO, and (c) Fe-Pd-GO. (d) XRD of S-Pd-GO and Fe-Pd-GO. The vertical grey lines indicate the peak position from the XRD simulation in (g). (e) SAED of the nanofilm. (f) Proposed structure of PdO square network in [001] projection with $a = b = 1$ nm (solid line) or $a = b = \frac{\sqrt{2}}{2}$ nm (dashed line). Simulated (g) XRD and (h) SAED from the structure in (f). Only XRD and SAED patterns from

hk0 are presented due to the nature of the thin nanofilm. (i) One of several proposed unit cells of PdO with face-centered cubic structure ($a = b = c = 1$ nm).

A crystal structure of the PdO square network is proposed (Figure 3f). The distance between adjacent palladium and oxygen atoms on the same plane perpendicular to the *c* axis is 0.5 nm, with $\alpha = \beta = \gamma = 90°$ and $a = b = 1$ nm (solid line) or $\frac{\sqrt{2}}{2}$ nm (dashed line). The peak positions from the XRD simulation accord well with the observation considering the peak dominance at 2θ of 26.1° from rGO (Figure 3d and g). The simulated SAED pattern perfectly matches the experimental results (Figure 3e and h). Due to the thin 2D nature (4.6 nm) and alignment perpendicular to the electron beam, the information on the *c* axis (*e.g.*, patterns other than *hk0*) is inconclusive. PdO can thus either be face-centered cubic ($a = b = c = 1$ nm, Figure 3i) or body-centered tetragonal ($a = b = \frac{\sqrt{2}}{2}$ nm). Although misfit of palladium crystals on graphene has been reported,[13] to the best of our knowledge there is no reported structure of palladium or palladium compounds when palladium is decorated on graphene. Six different space groups of palladium oxides have been reported: $Fm\bar{3}m$, I4/mmm, $P4_2/mmc$, $P4_2/mnm$, $Pm\bar{3}n$, and $Pn\bar{3}mS$.[31, 38-41] The proposed structure belongs to $Fm\bar{3}m$ (face-centered cubic) or I4/mmm (body-centered tetragonal), but the lattice spacing does not match the reported palladium oxides. The proposed structure is thus completely new for PdO.

The abiotic synthesis of the nanofilm can be extended to the synthesis of the same square network Fe-M-GO from other metals (M). As a demonstration, Fe-Ag-GO was synthesized when

$Na_2[PdCl_4]$ was replaced by $AgNO_3$. Surprisingly, Fe-Ag-GO, supposed to be a silver oxide (*e.g.*, $Ag_2O{\cdot}Ag_2O_3$), showed lattice spacing and interplanar angle (Figure 4a and b) identical to those in S-Pd-GO and Fe-Pd-GO. This type of silver oxide has not been reported before, and the data suggest that potentially a whole new class of metal oxide phase on rGO has been unveiled. GO can regulate crystal lattice after being decorated by nanoparticles.[13] In the present study, the Pd(II) ions and oxygen ions are possibly in the four positions of the rGO layer (Figure 4c), forming a square network that perfectly matches the PdO structure. The square network is possibly regulated by the dominant surface energy of rGO and not by the weak interaction between ions within PdO due to the large distance (minimum of 0.5 nm at the same layer, Figure 3f). Other metals can therefore also form the square network. Further investigations are in progress to detail the structure of Fe-Ag-GO and prepare a series of new square networks of other metal oxides.

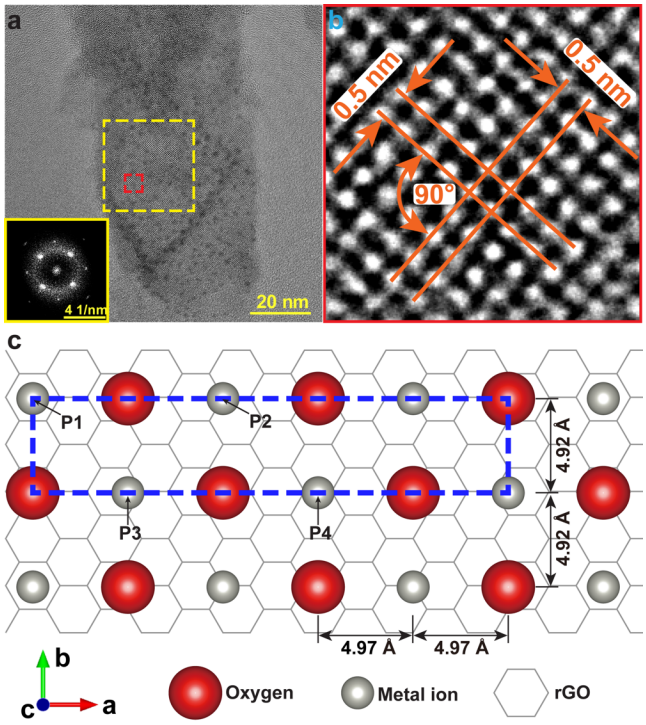

Figure 4. Morphology of Fe-Ag-GO and proposed model of lattice-matching between metal oxides and rGO. (a) TEM of Fe-Ag-GO. Inset: FFT of the yellow square area in (a). (b) HRTEM of the red square area in (a). (c) Metal ions and oxygen are in four positions (P1 – P4) of the rGO lattice. The blue box indicates a repeating unit.

In summary, we have reported a novel square network nanofilm of PdO on rGO from a microbial biosynthesis by *S. oneidensis* MR-1 combined with a hydrothermal process. The biogenic nanofilm originates from the interaction between GO and dissolved Pd(0) atoms (or atomic clusters) released from the periplasm of MR-1 cells during the hydrothermal process. An analogous bioinspired, abiotic synthesis produced the same structure and confirmed the essential role of dissolved Pd(0). A new crystal structure of the PdO phase was proposed, and an isomorphous nanofilm is obtained when $Na_2[PdCl_4]$ was replaced by $AgNO_3$ in the abiotic synthesis.

Graphene has been used in a wide range of sophisticated applications in electronics, energy storage, biomedicine, and photovoltaics.[42-45] Our present study shows that rGO can be combined with transition metal oxides into two-dimensional metal oxide/graphene composites. Superlattices of metal oxides on rGO can thus be produced using simple wet chemical synthesis. With the tremendous variety of transition metal electronic, catalytic, and other properties, the new graphene-based composites materials might therefore offer entirely novel perspectives for even more sophisticated electronic and other applications. The novel properties of the hybrids as well as their applications are currently being investigated and will be communicated in future reports.

ASSOCIATED CONTENT

Supporting Information.

The following files are available free of charge.

Experimental details, TEM, HRTEM, AFM, XRD characterizations of the products from control experiments, large-size HRTEM of PdO layer, synthesis scheme of control experiments, HRTEM of PdNPs, morphological evolution of the nanofilm, simulated XRD data (PDF)

AUTHOR INFORMATION

Corresponding Author

Feng Zhao – CAS Key Laboratory of Urban Pollutant Conversion, Institute of Urban Environment, Chinese Academy of Sciences, 1799 Jimei Road, Xiamen, 361021, China;

Email: fzhao@iue.ac.cn

Christian Engelbrekt – Department of Chemistry, Technical University of Denmark, Kemitorvet, Building 207, Kongens Lyngby, DK-2800, Denmark;

Email: cheng@kemi.dtu.dk

Xinxin Xiao – Department of Chemistry, Technical University of Denmark, Kemitorvet, Building 207, Kongens Lyngby, DK-2800, Denmark;

Email: xixiao@kemi.dtu.dk

Author Contributions

¶Deceased January 09, 2020.

Author Contributions

Z.Z. conceived and designed the study. F.Z., C.E., and X.X. supervised the study. Z.Z. performed the synthesis, TEM, HRTEM, AFM, and structural simulations. H.C. performed XRD and XPS experiments. J. M. performed STEM experiments. Z.Z., H.C., Y.X., J.U., F.Z., C.E., and X.X. were involved in the data interpretation, discussed the results, and commented on the study. Z.Z., X.X., and C.E. wrote the manuscript. J.Z. and X.X. provided financial support. All authors discussed the results and commented on the manuscript.

ACKNOWLEDGEMENTS

Financial support from the National Natural Science Foundation of China (22025603) and the China Scholarship Council (No. 201606130019) is greatly appreciated. X.X. acknowledges a Villum Experiment (grant No. 35844).

Notes

The authors declare no conflict of interest.

REFERENCES

(1) Lee, J.-H.; Kim, M.-G.; Yoo, B.; Myung, N. V.; Maeng, J.; Lee, T.; Dohnalkova, A. C.; Fredrickson, J. K.; Sadowsky, M. J.; Hur, H.-G., Biogenic formation of photoactive arsenic-sulfide nanotubes by *Shewanella* sp. strain HN-41. *Proc. Natl. Acad. Sci. U. S. A.* **2007,** *104*, 20410-20415.

(2) Hibble, S. J.; Chippindale, A. M.; Pohl, A. H.; Hannon, A. C., Surprises from a simple material—the structure and properties of nickel cyanide. *Angew. Chem. Int. Ed.* **2007,** *46*, 7116-7118.
(3) Allendorf, M. D.; Stavila, V., Crystal engineering, structure–function relationships, and the future of metal–organic frameworks. *CrystEngComm* **2015,** *17*, 229-246.
(4) Hollingsworth Mark, D., Crystal engineering: From structure to function. *Science* **2002,** *295*, 2410-2413.
(5) Sunku, S. S.; Ni, G. X.; Jiang, B. Y.; Yoo, H.; Sternbach, A.; McLeod, A. S.; Stauber, T.; Xiong, L.; Taniguchi, T.; Watanabe, K.; Kim, P.; Fogler, M. M.; Basov, D. N., Photonic crystals for nano-light in moiré graphene superlattices. *Science* **2018,** *362*, 1153-1156.
(6) Cao, Y.; Fatemi, V.; Fang, S.; Watanabe, K.; Taniguchi, T.; Kaxiras, E.; Jarillo-Herrero, P., Unconventional superconductivity in magic-angle graphene superlattices. *Nature* **2018,** *556*, 43-50.
(7) Chen, Z.-G.; Shi, Z.; Yang, W.; Lu, X.; Lai, Y.; Yan, H.; Wang, F.; Zhang, G.; Li, Z., Observation of an intrinsic bandgap and Landau level renormalization in graphene/boron-nitride heterostructures. *Nat. Commun.* **2014,** *5*, 4461.
(8) Ponomarenko, L. A.; Gorbachev, R. V.; Yu, G. L.; Elias, D. C.; Jalil, R.; Patel, A. A.; Mishchenko, A.; Mayorov, A. S.; Woods, C. R.; Wallbank, J. R.; Mucha-Kruczynski, M.; Piot, B. A.; Potemski, M.; Grigorieva, I. V.; Novoselov, K. S.; Guinea, F.; Fal'ko, V. I.; Geim, A. K., Cloning of Dirac fermions in graphene superlattices. *Nature* **2013,** *497*, 594-597.
(9) Krishna Kumar, R.; Mishchenko, A.; Chen, X.; Pezzini, S.; Auton, G. H.; Ponomarenko, L. A.; Zeitler, U.; Eaves, L.; Fal'ko, V. I.; Geim, A. K., High-order fractal states in graphene superlattices. *Proc. Natl. Acad. Sci. U. S. A.* **2018,** *115*, 5135.
(10) Berdyugin Alexey, I.; Xin, N.; Gao, H.; Slizovskiy, S.; Dong, Z.; Bhattacharjee, S.; Kumaravadivel, P.; Xu, S.; Ponomarenko, L. A.; Holwill, M.; Bandurin, D. A.; Kim, M.; Cao, Y.; Greenaway, M. T.; Novoselov, K. S.; Grigorieva, I. V.; Watanabe, K.; Taniguchi, T.; Fal'ko, V. I.; Levitov, L. S.*, et al.*, Out-of-equilibrium criticalities in graphene superlattices. *Science* **2022,** *375*, 430-433.
(11) Yankowitz, M.; Xue, J.; Cormode, D.; Sanchez-Yamagishi, J. D.; Watanabe, K.; Taniguchi, T.; Jarillo-Herrero, P.; Jacquod, P.; LeRoy, B. J., Emergence of superlattice Dirac points in graphene on hexagonal boron nitride. *Nat. Phys.* **2012,** *8*, 382-386.
(12) Wang, L.; Zihlmann, S.; Liu, M.-H.; Makk, P.; Watanabe, K.; Taniguchi, T.; Baumgartner, A.; Schönenberger, C., New Generation of Moiré Superlattices in Doubly Aligned hBN/Graphene/hBN Heterostructures. *Nano Lett.* **2019,** *19*, 2371-2376.
(13) Jeon, J.-M.; Kim, T. L.; Shim, Y.-S.; Choi, Y. R.; Choi, S.; Lee, S.; Kwon, K. C.; Hong, S.-H.; Kim, Y.-W.; Kim, S. Y.; Kim, M.; Jang, H. W., Microscopic evidence for strong interaction between Pd and graphene oxide that results in metal-decoration-induced reduction of graphene oxide. *Adv. Mater.* **2017,** *29*, 1605929.

(14) Liu, J.; Zheng, Y.; Hong, Z.; Cai, K.; Zhao, F.; Han, H., Microbial synthesis of highly dispersed PdAu alloy for enhanced electrocatalysis. *Sci. Adv.* **2016,** *2*, e1600858.
(15) Gracia-Espino, E.; Hu, G.; Shchukarev, A.; Wågberg, T., Understanding the interface of six-shell cuboctahedral and icosahedral palladium clusters on reduced graphene oxide: Experimental and theoretical study. *J. Am. Chem. Soc.* **2014,** *136*, 6626-6633.
(16) Gong, C.; Robertson, A. W.; He, K.; Ford, C.; Watt, A. A. R.; Warner, J. H., Interactions of Pb and Te atoms with graphene. *Dalton Trans.* **2014,** *43*, 7442-7448.
(17) Franz, D.; Schröder, U.; Shayduk, R.; Arndt, B.; Noei, H.; Vonk, V.; Michely, T.; Stierle, A., Hydrogen Solubility and Atomic Structure of Graphene Supported Pd Nanoclusters. *ACS Nano* **2021,** *15*, 15771-15780.
(18) Wu, R.; Tian, X.; Xiao, Y.; Ulstrup, J.; Molager Christensen, H. E.; Zhao, F.; Zhang, J., Selective electrocatalysis of biofuel molecular oxidation using palladium nanoparticles generated on *Shewanella oneidensis* MR-1. *J. Mater. Chem. A* **2018,** *6*, 10655-10662.
(19) Zheng, Z.; Xiao, Y.; Zhao, F.; Ulstrup, J.; Zhang, J., Bacterially generated nanocatalysts and their applications. In *Novel Catalyst Materials for Bioelectrochemical Systems: Fundamentals and Applications*, American Chemical Society: 2020; Vol. 1342, pp 97-122.
(20) Wu, X.; Zhao, F.; Rahunen, N.; Varcoe, J. R.; Avignone-Rossa, C.; Thumser, A. E.; Slade, R. C. T., A role for microbial palladium nanoparticles in extracellular electron transfer. *Angew. Chem. Int. Ed.* **2010,** *50*, 427-430.
(21) Lower Steven, K.; Hochella Michael, F.; Beveridge Terry, J., Bacterial recognition of mineral surfaces: Nanoscale interactions between *Shewanella* and α-FeOOH. *Science* **2001,** *292*, 1360-1363.
(22) Marsili, E.; Baron, D. B.; Shikhare, I. D.; Coursolle, D.; Gralnick, J. A.; Bond, D. R., *Shewanella* secretes flavins that mediate extracellular electron transfer. *Proc. Natl. Acad. Sci. U. S. A.* **2008,** *105*, 3968-3973.
(23) De Windt, W.; Boon, N.; Van den Bulcke, J.; Rubberecht, L.; Prata, F.; Mast, J.; Hennebel, T.; Verstraete, W., Biological control of the size and reactivity of catalytic Pd(0) produced by *Shewanella oneidensis*. *Antonie van Leeuwenhoek* **2006,** *90*, 377-389.
(24) Neal, A. L.; Bank, T. L.; Hochella, M. F.; Rosso, K. M., Cell adhesion of *Shewanella oneidensisto* iron oxide minerals: Effect of different single crystal faces. *Geochem. Trans.* **2005,** *6*, 77.
(25) Huang, J.; Lin, L.; Sun, D.; Chen, H.; Yang, D.; Li, Q., Bio-inspired synthesis of metal nanomaterials and applications. *Chem. Soc. Rev.* **2015,** *44*, 6330-6374.
(26) Kim, S.; Park, C. B., Bio-inspired synthesis of minerals for energy, environment, and medicinal applications. *Adv. Funct. Mater.* **2013,** *23*, 10-25.
(27) Velusamy, P.; Kumar, G. V.; Jeyanthi, V.; Das, J.; Pachaiappan, R., Bio-inspired green nanoparticles: Synthesis, mechanism, and antibacterial application. *Toxicol. Res.* **2016,** *32*, 95-102.

(28) Klem, M. T.; Willits, D.; Solis, D. J.; Belcher, A. M.; Young, M.; Douglas, T., Bio-inspired synthesis of protein-encapsulated CoPt nanoparticles. *Adv. Funct. Mater.* **2005,** *15*, 1489-1494.
(29) Samoylov, A. M.; Ivkov, S. A.; Pelipenko, D. I.; Sharov, M. K.; Tsyganova, V. O.; Agapov, B. L.; Tutov, E. A.; Badica, P., Structural changes in palladium nanofilms during thermal oxidation. *Inorg. Mater.* **2020,** *56*, 1020-1026.
(30) Orent, T. W.; Bader, S. D., LEED and ELS study of the initial oxidation of Pd(100). *Surf. Sci.* **1982,** *115*, 323-334.
(31) Kumar, J.; Saxena, R., Formation of NaCl- and Cu_2O-type oxides of platinum and palladium on carbon and alumina support films. *J. Less-Common Met.* **1989,** *147*, 59-71.
(32) Zheng, Z.; Xiao, Y.; Cao, H.; Tian, X.; Wu, R.; Zhang, J.; Ulstrup, J.; Zhao, F., Effect of copper and phosphate on the biosynthesis of palladium nanoparticles by *Shewanella oneidensis* MR-1. *ChemElectroChem* **2020,** *7*, 4460-4468.
(33) Windt, W. D.; Aelterman, P.; Verstraete, W., Bioreductive deposition of palladium (0) nanoparticles on *Shewanella oneidensis* with catalytic activity towards reductive dechlorination of polychlorinated biphenyls. *Environ. Microbiol.* **2005,** *7*, 314-325.
(34) Meyer, H. J.; Müller-Buschbaum, H., Eine neue durch oxidspuren stabilisierte form des palladiums. *J. Less-Common Met.* **1980,** *76*, 293-298.
(35) Ng, C. K.; Cai Tan, T. K.; Song, H.; Cao, B., Reductive formation of palladium nanoparticles by *Shewanella oneidensis*: role of outer membrane cytochromes and hydrogenases. *RSC Adv.* **2013,** *3*, 22498-22503.
(36) Yang, Z.-N.; Hou, Y.-N.; Zhang, B.; Cheng, H.-Y.; Yong, Y.-C.; Liu, W.-Z.; Han, J.-L.; Liu, S.-J.; Wang, A.-J., Insights into palladium nanoparticles produced by *Shewanella oneidensis* MR-1: Roles of NADH dehydrogenases and hydrogenases. *Environ. Res.* **2020,** *191*, 110196.
(37) Zheng, Z.; Xiao, Y.; Wu, R.; Mølager Christensen, H. E.; Zhao, F.; Zhang, J., Electrons selective uptake of a metal-reducing bacterium *Shewanella oneidensis* MR-1 from ferrocyanide. *Biosens. Bioelectron.* **2019,** *142*, 111571.
(38) Christy, A. G.; Clark, S. M., Structural behavior of palladium (II) oxide and a palladium suboxide at high pressure: An energy-dispersive x-ray-diffraction study. *Phys. Rev. B* **1995,** *52*, 9259-9265.
(39) Moore, W. J.; Pauling, L., The crystal structures of the tetragonal monoxides of lead, tin, palladium, and platinum. *J. Am. Chem. Soc.* **1941,** *63*, 1392-1394.
(40) Shaplygin, I.; Aparnikov, G.; Lazarev, V., Preparation of palladium dioxide at high-pressure. *Zh. Neorg. Khim.* **1978,** *23*, 884-887.
(41) Meyer, H. J.; Müller-Buschbaum, H., Ein beitrag zur chemie von verbindungen des bautyps $M_xPd_3O_4$ / A contribution to the chemistry of the compounds $M_xPd_3O_4$. *Z. Naturforsch., B: Chem. Sci.* **1979,** *34*, 1661-1662.
(42) Cao, H.; Zheng, Z.; Norby, P.; Xiao, X.; Mossin, S., Electrochemically induced phase transition in $V_3O_7 \cdot H_2O$ nanobelts/reduced graphene oxide composites for aqueous zinc-ion batteries. *Small* **2021,** *17*, 2100558.

(43) Yoon, H. J.; Kim, T. H.; Zhang, Z.; Azizi, E.; Pham, T. M.; Paoletti, C.; Lin, J.; Ramnath, N.; Wicha, M. S.; Hayes, D. F.; Simeone, D. M.; Nagrath, S., Sensitive capture of circulating tumour cells by functionalized graphene oxide nanosheets. *Nat. Nanotechnol.* **2013,** *8*, 735-741.
(44) Guo, C. X.; Yang, H. B.; Sheng, Z. M.; Lu, Z. S.; Song, Q. L.; Li, C. M., Layered graphene/quantum dots for photovoltaic devices. *Angew. Chem. Int. Ed.* **2010,** *49*, 3014-3017.
(45) Li, H.; Pang, S.; Wu, S.; Feng, X.; Müllen, K.; Bubeck, C., Layer-by-layer assembly and UV photoreduction of graphene–polyoxometalate composite films for electronics. *J. Am. Chem. Soc.* **2011,** *133*, 9423-9429.

Table of contents

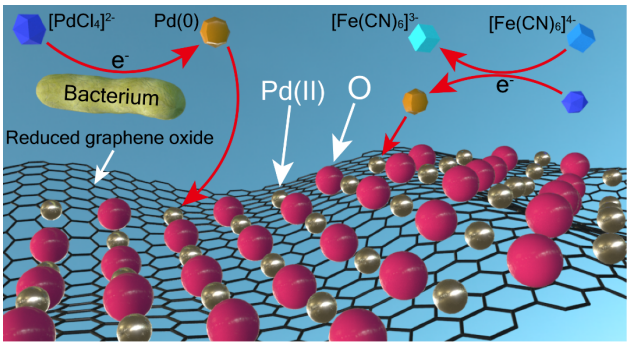

For Table of Contents Only